Final Report of the Air Force Project (FA4869-06-1-0078)
REF: AOARD-06-4073
Title: Multi-channel ZnO nanoconductors with tunable optoelectrical properties
Dr. Chuan-Pu Liu, National Cheng Kung University, Tainan, Taiwan

1. Al:ZnO nanowires

We have developed a new doping technology for controlled growth recently. Successful doping of ZnO nanomaterials is still a challenge even today due to the vapor pressure difference by orders of magnitudes between dopants and Zn and the reports of successful doping are scarce. We have used our proposed alloying evaporation deposition (AED) method [1] to synthesize Al doped ZnO nanowires with various doping concentrations. The atomic ratio of Al/(Al+Zn) in nanowires could range from 0 to 3.7 at.% determined by electron energy loss spectroscopy. Fig. 1(a) shows the Al map of Al:ZnO nanowires with the doping concentration around 3.7 at.%. The corresponding electron diffraction patterns confirm the nanowires are hexagonal wurtzite-structured ZnO as shown in fig.1 (b). From the cathodoluminescence result, a strong ultraviolet (UV) band emission at 365~366 nm is shown in fig.1 (c). The UV emission shifts to a higher energy of around 3.37 eV compared with 3.29 eV from the pure ZnO nanowires [2] is attributed to Al incorporation.

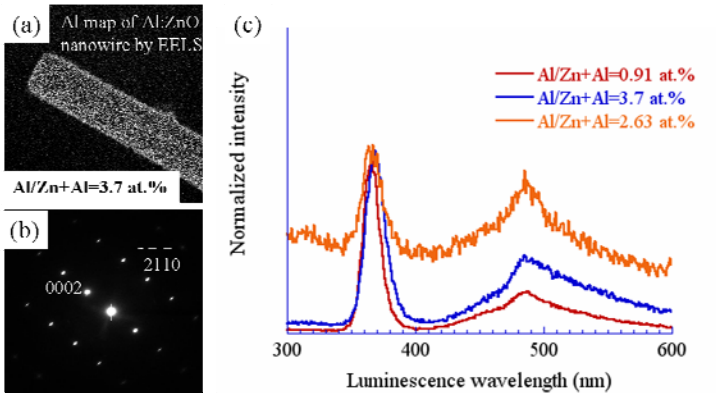

Fig. 1(a) Al map of Al:ZnO nanowires with the doping concentration around 3.7 at.%. (b) Corresponding electron diffraction patterns of the nanowires in (a) and (c) Cathodoluminescence spectra of Al:ZnO nanowires.

2. Al: ZnO rectangular nanorods

Besides, we provide another interesting route of fabricating Al: ZnO rectangular

Report Documentation Page

Form Approved
OMB No. 0704-0188

1. REPORT DATE	2. REPORT TYPE	3. DATES COVERED
06 DEC 2007	**Final**	**05-06-2006 to 04-06-2007**

4. TITLE AND SUBTITLE
Multi-channel ZnO nanoconductors with tunable opto-electrical properties

5a. CONTRACT NUMBER
FA48690610078

5b. GRANT NUMBER

5c. PROGRAM ELEMENT NUMBER

6. AUTHOR(S)
Chuan-Pu Liu

5d. PROJECT NUMBER

5e. TASK NUMBER

5f. WORK UNIT NUMBER

7. PERFORMING ORGANIZATION NAME(S) AND ADDRESS(ES)
National Cheng-Kung University,1 University Road,Tainan, Taiwan,TW,N/A

8. PERFORMING ORGANIZATION REPORT NUMBER
N/A

9. SPONSORING/MONITORING AGENCY NAME(S) AND ADDRESS(ES)
AOARD, UNIT 45002, APO, AP, 96337-5002

10. SPONSOR/MONITOR'S ACRONYM(S)
AOARD-064073

11. SPONSOR/MONITOR'S REPORT NUMBER(S)

12. DISTRIBUTION/AVAILABILITY STATEMENT
Approved for public release; distribution unlimited

13. SUPPLEMENTARY NOTES

14. ABSTRACT

A new doping technology for controlled growth has been developed recently. Successful doping of ZnO nanomaterials is still a challenge even today due to the vapor pressure difference by orders of magnitudes between dopants and Zn and literature reports of successful doping are scarce. The alloying evaporation deposition (AED) method was used to synthesize Al doped ZnO nanowires with various doping concentrations. Several types of single-crystalline Zn and Zn/ZnO core-shell polyhedrons were synthesized step by step by CVD followed by designed oxidizing treatments. Direct evidences of apparent deformation of polyhedrons after stress relief were provided to prove the lattice mismatch effect. Room-temperature CL measurements show the polyhedrons exhibit tunable UV and green emissions with different oxidation conditions, which were attributed to surface and strain effects. The Zn/ZnO polyhedrons are promising for opto-electronic nanodevice applications.

15. SUBJECT TERMS

16. SECURITY CLASSIFICATION OF:			17. LIMITATION OF ABSTRACT	18. NUMBER OF PAGES	19a. NAME OF RESPONSIBLE PERSON
a. REPORT	b. ABSTRACT	c. THIS PAGE			
unclassified	**unclassified**	**unclassified**	**Same as Report (SAR)**	**10**	

nanorods by doping induced composition fluctuations. The rectangular nanorods are nucleated from a sheet-like nanostructure with periodic thickness fluctuations resulting from doping concentration modulation. Figure 2(a) is a low-magnification scanning electron microscopy (SEM) image showing nanowires as well as arrays of rectangular nanorods synthesized on a silicon substrate. A typical array of Al: ZnO rectangular nanorods is shown in a higher magnification SEM image in Figure 2(b). This structure exhibits rare four-fold or two-fold symmetry instead of the common six-fold symmetry of ZnO. An entire view of the rectangular nanorod arrays is shown in the inset of Figure 2(b). Figure 2(c) shows the root part of the Al:ZnO rectangular nanorods, which are connected to one another with thin sheets. The morphology of the arrays of the rectangular nanorods is distinct from comb-like structures.

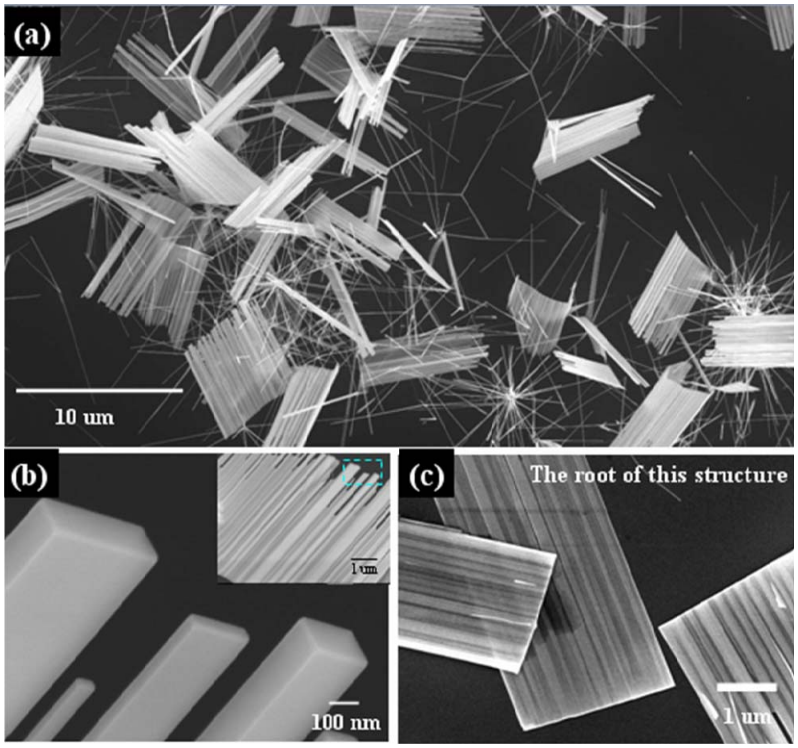

Fig. 2. SEM images of (a) the as-synthesized Al: ZnO rectangular nanorods grown on a Si substrate; (b) the upper regions of the rods with the inset for an entire view of the rectangular nanorod array, (c) the root of the rectangular nanorod arrays.

Fig. 3(a) shows a low-magnification transmission electron microscopy (TEM) image of the Al: ZnO rectangular nanorod arrays. The uniform contrast indicates uniform thickness over individual nanorods. A corresponding diffraction pattern in Fig. 3(b) reveals that the rectangular nanorods are single-crystalline wurtzite structure growing along the c-axis, while the top and side facets are $(2\bar{1}\bar{1}0)$ and (0002) planes, respectively. A HRTEM image of the interface region of a rectangular nanorod and

contiguous nanosheet is shown in Fig. 3(c). The lattice constant of the rectangular nanorod and nanosheet is 5.10 Å and 5.12 Å, respectively. Besides, there are obvious lattice distortions and dislocations near the interface region as shown in the dashed circles. The energy-dispersive x-ray spectrum in the inset of Fig. 3(c) shows that the rectangular nanorods consist of Zn, O, and Al. In addition, the atomic ratio of Al to (Al+Zn) in the ZnO rectangular nanorods and nanosheets calculated from the TEM EDX results is around 2.10 and 1.52 at.%, respectively. Apparently, the lattice distortions, dislocations, and differences in lattice constant are caused by the difference in Al concentration of rectangular rods and intermediate nanosheets.

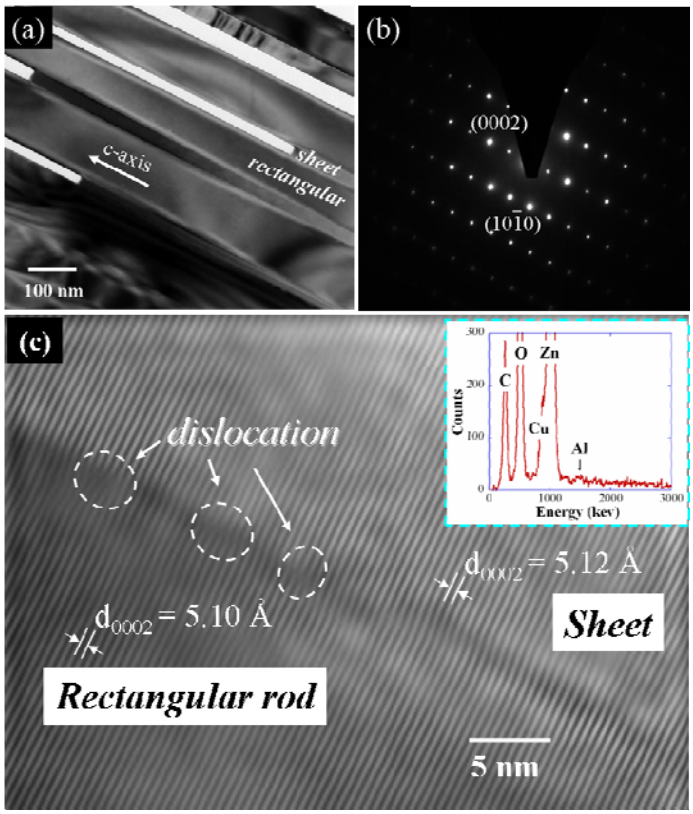

Fig. 3. (a) A low-magnification bright-field TEM image of an array of Al: ZnO rectangular nanorods with (b) the corresponding electron diffraction pattern; (c) high-resolution TEM image, after Fourier filter, showing the dislocations at the interface of the sheet and rectangular nanorod with the inset for the energy dispersive x-ray spectrum of the rectangular nanorod.

The arrays of single-crystalline Al: ZnO rectangular nanorods were synthesized at 650 ^{o}C by the proposed AED method. The nanostructures started with the growth of single-crystalline ZnO nanobelts with periodic thickness and Al concentration modulation. A three-stage growth process was proposed for the Al: ZnO rectangular nanorods. The first stage involved the growth of the nanobelt along the [01 $\bar{1}$ 0]

direction. Secondly, Al dopants tend to redistribute due to the high diffusion rate at high temperature to reduce the overall lattice strain induced by Al doping, resulting in doping concentration modulation along the length direction of the sheet-like structure [3]. The regions with higher Al concentration are energetically favorable for higher deposition rate of ZnO and larger local thickness. Thus, an Al:ZnO nanosheet with periodic thickness variations was consequently formed. Lastly, the rod-like parts with higher thickness and Al concentration continuously grew along the c-axis out of the sheets and developed into arrays of rectangular rods. The composition modulation induced by doping may serve as a driving force for creating more interesting nanostructures with tunable properties.

3. **Two Types Luminescence Emitted from Opposite Sides of a Single ZnO Nanorod**

In addition, we demonstrate a simple method to fabricate ZnO nanorods, which exhibit ultraviolet emitted from one side and green light from the other side by the proposed AED methods. The fantastic luminescence phenomenon was attributed to varied concentration of oxygen vacancy at the two opposite sides of a single ZnO nanorod.

The room-temperature cathodoluminescence spectrum of the ZnO nanorods in Fig. 4 shows a relatively strong and sharp UV emission centered at 377 nm and broad green emission at around 500 nm. The ultraviolet emission is attributed to the near band edge excitonic emission of ZnO, while the green emission may be a result of the transition between the photoexcited holes and singly ionized oxygen vacancies.[4]

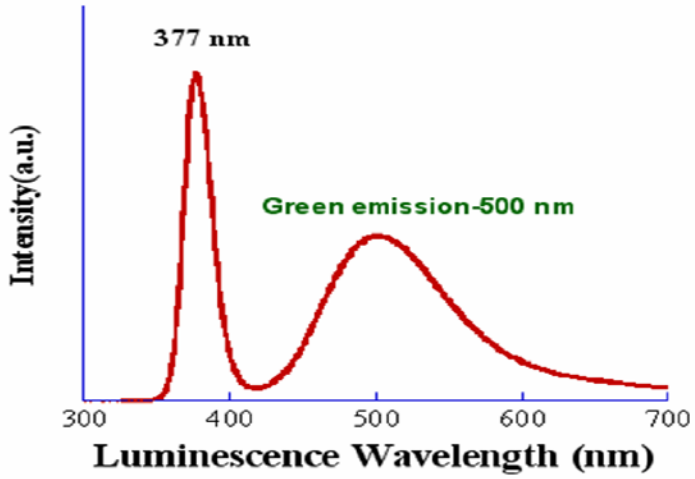

Fig. 4. Room-temperature cathodoluminescence spectrum of two-sided ZnO nanorods.

Two sides of ZnO nanorods emitting light at different wavelength are shown in Fig. 5. Figure 5(a) shows the CL microscopic image taken under the stimulation of 377 nm. It is interesting that enhancement of near band edge emission can be observed at the tips of the nanorods and the stronger green CL emission of the root than the tip of nanorods is shown in Fig. 5(b). Figure 5(c) shows the simulated image of two type luminescence in the ZnO nanorods. The green and blue segments represent green emission and near band edge emission of ZnO, respectively. The images demonstrate that the strong UV and green emissions distribute mainly at opposite sides of a single nanorod, indicating different concentration of oxygen vacancies relating to different Al doping.

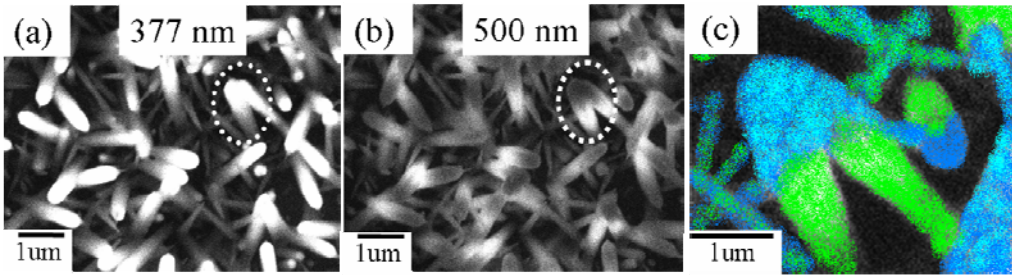

Fig. 5 CL microscopic images taken under the stimulation of (a) 377 nm and (b) 500 nm. (c) Simulated image of the luminescence in ZnO nanorods.

Fig. 6(a) shows low-magnification TEM bright-field image of the ZnO nanorod. The uniform contrast indicates uniform thickness over individual nanorods. The chemical stoichiometry of the ZnO nanorods examined with energy dispersive spectrum in high-resolution TEM affirms that the atomic ratio of Zn:O on the tip and root of a nanorod is around 48.7: 51.3 and 52.4: 47.6, respectively. The difference in oxygen concentration exceeds 3.7 at.% between two ends of the ZnO nanorod. Figure 6(b) is a high-resolution TEM image from the outlined region indicated in Fig. 6(a). The corresponding diffraction pattern (the inset in Fig. 6(b)) reveals that the nanorod is single-crystalline wurtzite structure growing along the c-axis.

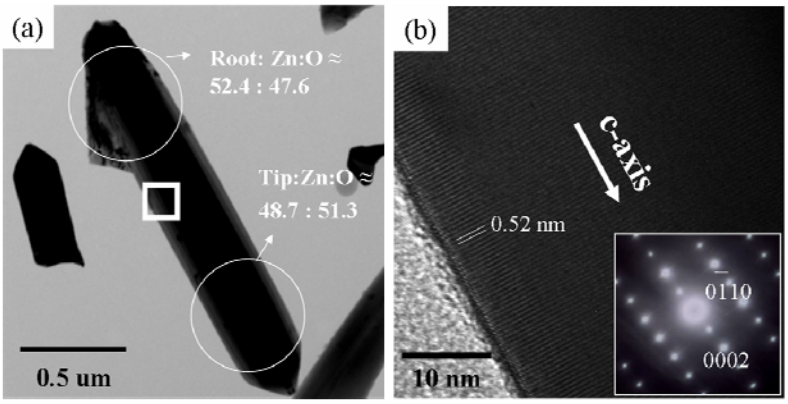

Fig. 6 (a) An TEM bright field image of a ZnO nanorod; (b) High-resolution TEM image of the ZnO nanorod from the box marked in Fig. 6(a) with the inset for the corresponding selected-area electron diffraction pattern of the nanorod.

The variation in stoichometry is attributed to the alloying of Al/Zn mixed sources during the growth of nanorods. The Al vapor pressure is much lower than Zn by 10^{-12} order at the same temperature range. However, Zn and Al sources in the process would form a certain quantity of Zn–Al alloy by interdiffusion through the Zn/Al interface. Since the bond energy of Zn- Al is higher than Zn-Zn (Zn-Al: 0.101 eV; Zn-Zn: 0.054 eV) [5], which may cause the decreasing of Zn vapor pressure in the quartz tube with the alloying of Zn and Al during the synthesis of nanorods. In contrast, the flow rate of oxygen in the furnace is invariant. Consequently, the tip of ZnO nanorods exhibits lower zinc concentration than the root. The roots of nanorods with higher zinc and lower oxygen concentration exhibiting green emission is attributed to the existence of oxygen vacancy. The schematic diagram in Fig. 7 shows the different steps of source transformation during the growth of ZnO nanorods.

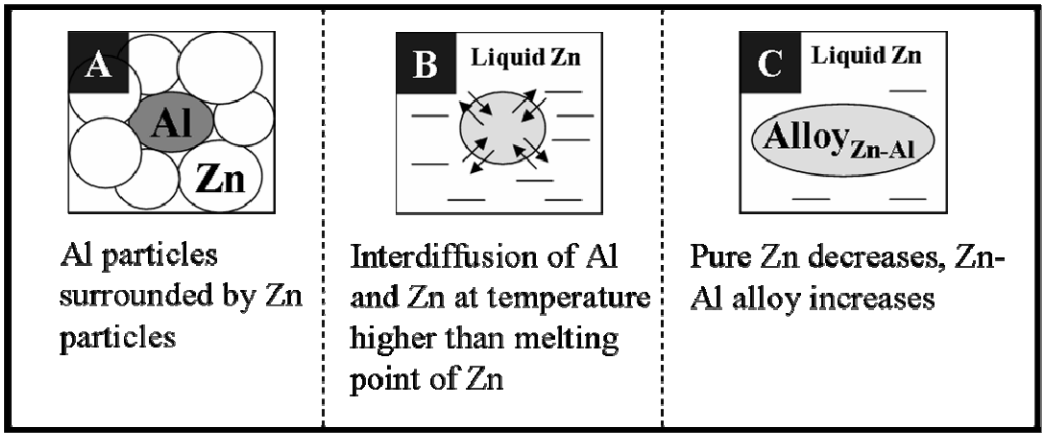

Fig. 7. Schematic illustration of different steps of source transformation during the growth of ZnO nanorods.

The process provides a simple method to adjust optical properties in a single nanorod by one step process, and shows promising potential for developing nano-pixel optoelectronics.

4. Various Single-crystalline Zn and Zn/ZnO Core-shell Polyhedrons with Tunable Photoemission

The Zn single-crystalline polyhedral, Zn/ZnO core-shell hexagonal polyhedrons,

ZnO shelled structures as shown in Fig.8 (a) were synthesized by chemical vapor deposition followed by different annealing treatments. The core-shell polyhedrons started with the growth of single-crystalline Zn polyhedrons, nucleated on a Si substrate and the ZnO layers were formed on the surface of the Zn polyhedrons upon the oxidation treatments (shown in Fig. 8(b)). The thickness of the oxide layers can be controlled precisely by adjusting the temperature and O_2/Ar ratio during the annealing process.

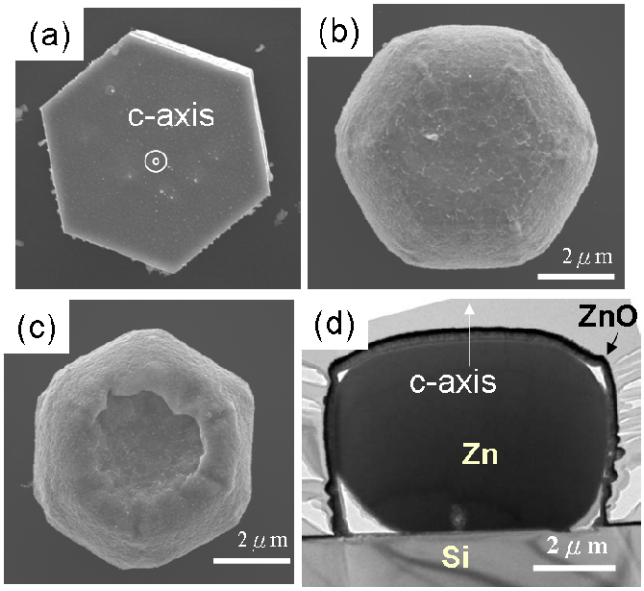

Fig.8: SEM images of (a) Zn polyhedron (b) Zn/ZnO core-shell polyhedron (c) ZnO shelled structure after annealing at 400, 450, and 500 ^{o}C, respectively, for an hour (d) TEM image of the cross-section of Zn/ZnO core-shell polyhedrons.

The micro-sized single-crystalline Zn polyhedrons formed on Si in spite of a large lattice mismatch between Zn and Si has been attributed to the higher strain tolerance of the metal bonds of Zn compared with the ionic/covalent bonds of ceramic ZnO. Figure 9(a) is the cross-sectional SEM image of a polyhedron upon annealing at 500°C, showing a crack at the interface as indicated, which may be ascribed to the difference in thermal expansion coefficient. However, the crack becomes larger and propagates along the interface after the half of the polyhedron has been sliced by focus ion beam, as shown in figure 9(b), due to less restriction from the surrounding materials. Furthermore, the TEM image in figure 9(c) shows complete detachment of the polyhedron after a TEM thin foil has been made. More interestingly, polyhedrons underwent morphology deformation during the slicing process and the height/ width ratio of the polyhedron is increased from 0.60 in figure 9(b) to 0.71 in figure 9(c), conforming a large degree of strain restored resulting from the lattice mismatch of

Zn/Si and Zn/ZnO. The results provide direct evidences in the formation of epitaxial micro/nano structures by lattice strain. In this core-shell Zn/ZnO polyhedrons on Si, if the annealing temperature is below 500°C, the ZnO thickness is too thin to affect the Zn/Si interface, so that the ZnO shell tends to detach from the rounded Zn polyhedron. On the other hand, when the annealing temperature is higher than 500°C, the ZnO thickness is thick enough to beak down the Zn/Si interface, causing collapse on top and detachment on bottom of a polyhedron. Figure 9(d) shows the schematic diagrams of the formation and deformation of Zn/ZnO core-shell polyhedrons.

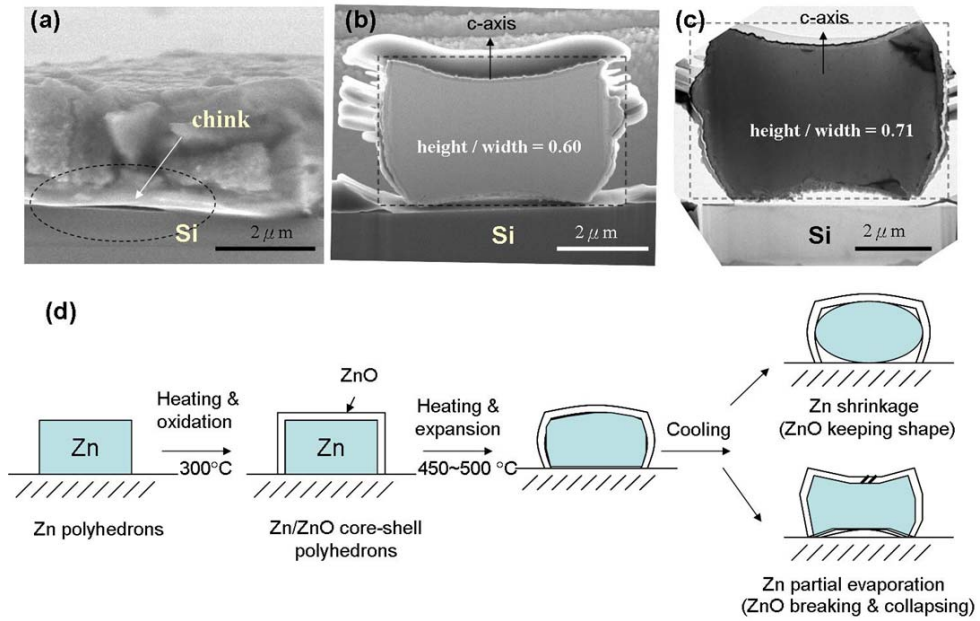

Fig.9 Cross-sectional images of Zn/ZnO core-shell polyhedrons at different stages: (a) SEM image of a Zn/ZnO core/shell polyhedron before FIB slicing; (b) SEM image of another Zn/ZnO polyhedron being sliced in half by FIB; (c) TEM bright-field image of the Zn/ZnO polyhedron as in (b); (d) schematic diagram of the proposed formation mechanism of Zn/ZnO core-shell polyhedrons.

Fig. 10 is the room-temperature cathodoluminescence spectra of Zn/ZnO polyhedrons after annealing at different temperature, which exhibit tunable ultraviolet emissions and controllable green emissions with different oxidation conditions. The ultraviolet emissions shift to larger wavelength from 364 nm to 369 nm as the annealing temperature increases from 400°C to 550 °C.

We thus synthesis several types of single-crystalline Zn and Zn/ZnO core-shell polyhedrons synthesized step by step by CVD followed by designed oxidizing treatments. Direct evidences of apparent deformation of polyhedrons after stress relief were provided to prove the lattice mismatch effect. Room-temperature CL

measurements show the polyhedrons exhibit tunable UV and green emissions with different oxidation conditions, which were attributed to surface and strain effects. The Zn/ZnO polyhedrons are promising for opto-electronic nanodevice applications.

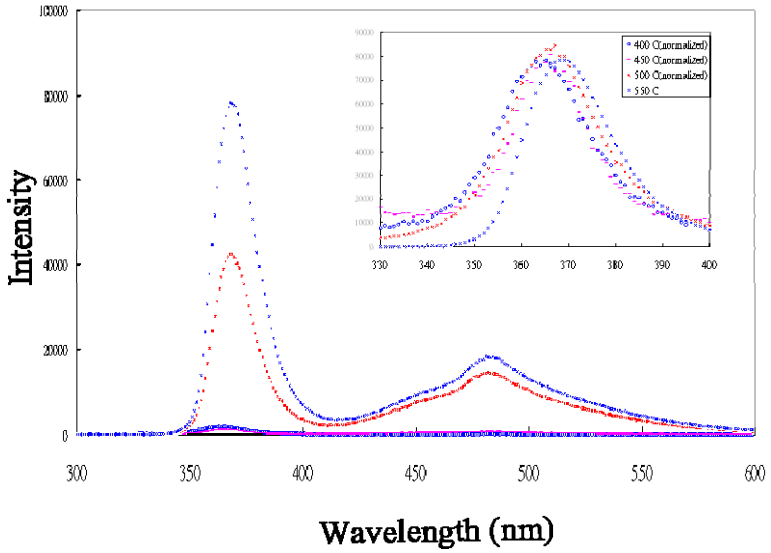

Fig. 10 Room-temperature CL spectra of the Zn/ZnO core-shell polyhedrons after annealing at different temperature with the inset for an enlarged view of UV emissions

References

[1] R. C. Wang, C. P. Liu, and J. L. Huang, Appl. Phys. Lett. **88**, 023111 (2006).

[2] R. C. Wang, C. P. Liu, J. L. Huang and S. J. Chen, Appl. Phys. Lett. **86**, 251104 (2005).

[3]P. J. Perrah, A. C. Chen, A. M. Moy, K. C. Hsieh and K. Y. Cheng J. Quant. Electron. **30**, 608 (1994).

[4] K. Vanhausden, W. L. Warren, C. H. Seager, D. R. Tallant, J. A. Voigt, and B. E. Gnade, J. Appl. Phys. **79**, 7983 (1996).

[5] M. Iqbal, M. A. Shaikh, J. I.Akhter, M.Ahmad,; M. Akhtar, M. J.Moughal, J. mater. science. **39**, 4255 (2004).

Publications

1. Chien-Lin KuO, Ruey-Chi Wang, Chuan-Pu Liu*, and Jow-Lay Huang, 'Composition Fluctuation Induced Growth of Al:ZnO Rectangular Nanorod Arrays', submitted to Nanotechnology in July 2007.

2. Wei- Yu Chen, Ruey- Chi Wang, and Chuan- Pu Liu*, 'Substrate Effect Induced Growth of Various Single-crystalline Zn and Zn/ZnO Core-shell Polyhedrons with Tunable Photoemission', submitted to Advanced Functional Materials in July 2007.

3. Chien-Lin KuO, Ruey-Chi Wang, Chuan-Pu Liu*, and Jow-Lay Huang, 'Two Emissions with Different Wavelength from Opposite Sides of a Single ZnO Nanorod', in preparation.